Inorganic Chemistry

ARTICLE

pubs.acs.org/IC

Chlorodifluoroacetyl Cyanide, $ClF_2CC(O)CN$: Synthesis, Structure, and Spectroscopic Characterization

Luis A. Ramos,[†] Sonia E. Ulic,[†,‡] Rosana M. Romano,[†] Shengrui Tong,[∥] Maofa Ge,[∥] Yuri V. Vishnevskiy,[⊥] Raphael J. Berger,[⊥] Norbert W. Mitzel,[⊥] Helmut Beckers,[§] Helge Willner,[§] and Carlos O. Della Védova*[,†,#]

[†]CEQUINOR (UNLP−CONICET), Departamento de Química, Facultad de Ciencias Exactas, Universidad Nacional de La Plata, 47 esq. 115, 1900 La Plata, República Argentina

[‡]Departamento de Ciencias Básicas, Universidad Nacional de Luján, Rutas 5 y 7 (6700) Luján, Argentina

[§]Fachbereich C - Anorganische Chemie, Bergische Universität Wuppertal, 42097 Wuppertal, Germany

[∥]State Key Laboratory for Structural Chemistry of Unstable and Stable Species, Institute of Chemistry, Chinese Academy of Sciences, Beijing 100190, China

[⊥]Universität Bielefeld, Lehrstuhl für Anorganische Chemie und Strukturchemie, Universitätsstraße 25, 33615 Bielefeld, Germany

[#]Laboratorio de Servicios a la Industria y al Sistema Científico (UNLP−CIC−CONICET), Buenos Aires, República Argentina

Supporting Information

ABSTRACT: The novel molecule difluorochloroacetyl cyanide, $ClF_2CC(O)CN$, has been characterized by IR (gas phase, Ar matrix), Raman (liquid), ^{19}F and ^{13}C NMR, and photoelectron (PES) spectroscopies; photoionization mass spectrometry (PIMS); and gas electron diffraction (GED). The conformational properties of $ClF_2CC(O)CN$ have been studied by joint application of vibrational spectroscopy, GED, and quantum chemical calculations. The existence of two conformers is detected in the gas and liquid phases, in which the C−Cl bond adopts *gauche* and *syn* orientations with respect to the C═O group. The computed enthalpy difference is in harmony with the experimental results of the *gauche* being more stable than the *syn* conformer by $\Delta H^\circ = 1.3$ kcal mol^{-1} (MP2/cc-pVTZ). The valence electronic properties and the possible ionization and dissociation processes of the title compound are studied using the PES and PIMS. The experimental first vertical ionization energy of 12.0 eV corresponds to the ejection of an electron of the oxygen lone pairs. Taking into account the properties and broad applications of acyl cyanides, $ClF_2CC(O)CN$ is a promising new precursor in preparative chemistry.

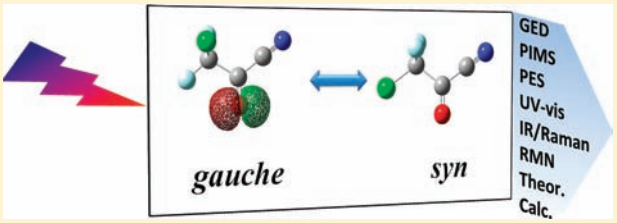

INTRODUCTION

Acyl and aryl cyanides have been widely studied as precursors in preparative chemistry.[1−5] They are useful acylating agents like the corresponding halides, with the advantage that auxiliary bases are not needed, due to the low acidity of the hydrocyanic acid formed. Reduction reactions of carbonyl cyanides constitute a valuable method for the formation of carbon−carbon bonds; this can be used to obtain biologically active molecules such as 1, 2-diketones[6] and other derivates. The reaction pathways have been found to be highly dependent on the conditions and the reducing agents, leading to cyanohydrins, dicyanohydrins, amine alcohols, etc.[7−10]

Even more, acyl cyanides have been used in multiple-component condensation reactions in the production of modern drugs.[11] The condensation of acyl cyanides with isonitriles and carboxylic acids affords β-amino acid diamides and related β-peptide analogues, which have been demonstrated to have antimicrobial properties.[12,13] More recently, the inter- and intramolecular cyanoesterification of unsaturated compounds has been developed. This allows the simultaneous introduction of cyano and other groups by direct cleavage of C−CN bonds followed by the addition of the unsaturated molecules. This procedure affords—with good regio- and stereoselectivities—highly substituted acrylonitriles, which constitute building blocks for the synthesis of different compound classes such as lactones, amino acids, and dicarboxylic acid derivates.[14−17] In addition, some acyl cyanides such as $CF_3C(O)CN$[18] are useful precursors of the carboxylic acids cyanide dimers, which also exhibit further applications in preparative chemistry.[19] Further examples of the high reactivity of carbonyl cyanides have also been reported in organometallic chemistry.[20,21]

Theoretical studies predict a planar CC(O)CN moiety. The electronic properties of these molecules analyzed by photoelectron spectroscopy showed that the first potential ionization energies correspond mainly to nonbonding orbitals at the oxygen atom and π-type bonding orbitals of the nitrile group.[22,23]

Received: June 29, 2011
Published: August 26, 2011

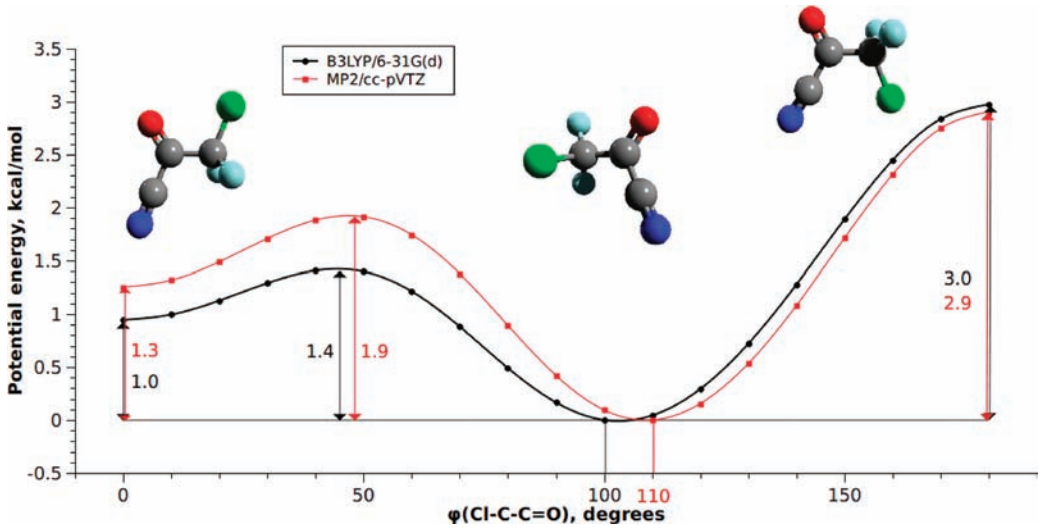

Figure 1. Theoretical potential energy curves for the internal rotation around the C2−C5 bond in $ClF_2CC(O)CN$ calculated at the MP2/cc-pVTZ (red line) and the B3LYP/6-31G(d) (black line) levels of theory. The double arrows indicate the relative energy (ΔE) of the *syn* form and energy barriers for the mutual *syn*−*gauche* interconversion (in kcal mol^{-1}), respectively.

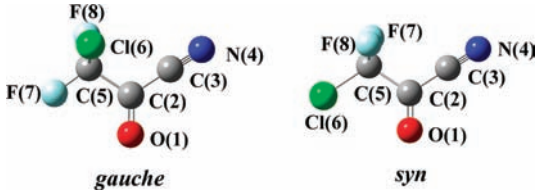

Figure 2. The *gauche* and *syn* conformations of $ClF_2CC(O)CN$ and labeling of the atoms used therein.

Taking into account the applicability of acyl cyanides as precursors and their relevant inherent properties, the synthesis and full characterization of the novel chlorodifluoroacetyl cyanide $ClF_2CC(O)CN$ is presented in this work. Its structure, conformational, and electronic properties are evaluated by a joint application of experimental and theoretical methods.

RESULTS AND DISCUSSION

General Properties. Solid $ClF_2CC(O)CN$ melts at −75 °C to a colorless liquid. The vapor pressure of the liquid was measured over a temperature range between −60 and 0 °C. Its temperature dependence can be described by eq 1, from which a boiling point of 35 °C was extrapolated. $ClF_2CC(O)CN$ is stable as a gas and a liquid at room temperature.

$$\ln(p) = -4809(1/T) + 12.98 \quad (p \text{ in atm}, T \text{ in K}) \qquad (1)$$

The ^{19}F NMR spectrum shows a singlet at $\delta = -69.5$ ppm attributed to both fluorine atoms of the $ClCF_2$ group (Figure S1, Supporting Information). The ^{13}C NMR spectrum exhibits two triplet signals at $\delta = 159.4$ ppm ($^2J_{(C-F)} = 40.3$ Hz) and $\delta = 118.2$ ppm ($^1J_{(C-F)} = 301.1$ Hz) and a singlet at 109.6 ppm, corresponding to the carbon atoms of the C═O, $ClCF_2$, and CN groups, respectively (Figure S1, Supporting Information). These values are in good agreement with those reported for similar compounds.[24] The UV−visible spectrum of gaseous $ClF_2CC(O)CN$ (Figure S2, Supporting Information) shows a structured absorption band (due to vibronic coupling) at $\lambda_{max} = 318$ nm attributed to the $n \rightarrow \pi^*$ transition located on the CO group and the decay of a stronger absorption at $\lambda_{max} < 190$ nm, which could be due to the $\pi_{CN} \rightarrow \pi_{CO}^*$ transition, according to those reported for similar molecules.[25]

Table 1. Calculated Relative Energies (ΔE, kcal mol^{-1}), Gibbs Free Energies (ΔG, kcal mol^{-1}) for the *syn* Conformer Relative to *gauche* $ClF_2CC(O)CN$, and Their Population at 298 K Calculated from Estimated ΔG Values Assuming a Boltzmann Distribution

method	$\Delta E°$	$\Delta G°$	*gauche* (%)	*syn* (%)
B3LYP/6-311+G(d)	1.11	0.90	90	10
B3LYP/6-311+G(3df)	1.18	0.94	91	9
MP2/6-311+G(d)	0.91	0.73	87	13
MP2/cc-pVTZ	1.26	1.04	92	8
CBS-QB3	0.83	0.61	85	15

Quantumchemical Calculation. The presence of the chlorine atom in $ClF_2CC(O)CN$ raises the possibility to adopt more than one orientation around the C−C(O) bond. To evaluate the expected conformational equilibrium, potential energy curves for the internal rotation about this bond were calculated at the B3LYP/6-31G(d) and MP2/cc-pVTZ levels of theory (Figure 1). In addition, full optimizations of all possible conformers on the potential energy surface of $ClF_2CC(O)CN$ were carried out using *ab initio* (MP2), DFT (B3LYP), and CBS-QB3 levels of theory. Two conformers, denoted as *gauche* (ϕ = (ClC−C(O)) ≈ 105°; C_1 symmetry) and *syn* (ϕ = (ClC−C(O)) ≈ 0°; C_s symmetry) (Figure 2), were found to be minimum energy structures. The calculated energies of both conformers and their estimated abundances are given in Table 1. The *gauche* conformer was predicted to be more stable than the *syn* form at all levels of theory. The energy differences, however, vary from 0.8 kcal mol^{-1} (CBS-QB3) to 1.3 kcal mol^{-1} (MP2/cc-pVTZ). A contribution of 15% of the *syn* conformer can be estimated for the gas phase at 298 K, according the calculated

dx.doi.org/10.1021/ic201390h |*Inorg. Chem.* 2011, 50, 9650–9659

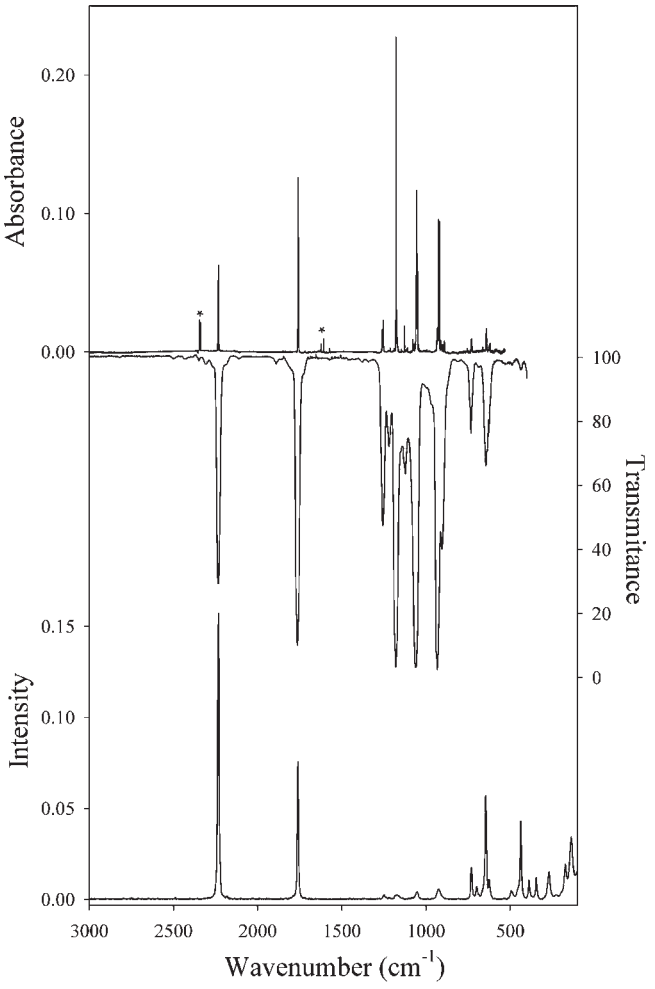

Figure 3. Upper trace: IR spectrum of $ClF_2CC(O)CN$ isolated in an Ar matrix at 16 K (resolution: 0.25 cm^{-1}). Middle trace: IR spectrum of gaseous $ClF_2CC(O)CN$ at 298 K (resolution: 2 cm^{-1}). Lower trace: Raman spectrum of liquid $ClF_2CC(O)CN$ at 298 K (resolution: 2 cm^{-1}). Bands due to impurities are marked by asterisks.

Gibbs free energy difference between the two forms (ΔG = 0.61 kcal mol^{-1}) at the CBS-QB3 level.

Additionally, two conformers with the F−C or Cl−C bonds in an *anti* position with respect to the C═O double bond have proven to be maxima on the potential hypersurface (one imaginary frequency), which is probably due to the repulsive interactions of F−C or Cl−C with the CN group. The remarkable low energy barrier for the *syn* → *gauche* interconversion (Figure 1) agrees well with the conformational results of the matrix isolation experiments described below.

Vibrational Spectra. Gas-phase IR, Ar-matrix IR, and Raman (liquid) spectra of $ClF_2CC(O)CN$ are shown in Figure 3. The observed vibrational frequencies are listed in Table 2 and compared with the calculated frequencies of the two possible conformers at the B3LYP/6-311+G(3df) level of theory. $ClF_2CC(O)CN$ has 18 fundamental vibrational modes which are expected to be active in IR and Raman.

The most intense band in the Raman spectrum appeared at 2232 cm^{-1} and was assigned to the stretching mode of the cyano group, ν(CN). This band was also observed as an intense absorption in the IR spectra (2233 cm^{-1}). This is contrary to the situation in carbonyl thiocyanates XC(O)SCN,[26] where ν(CN) is the strongest band in the Raman spectrum but has no counterpart in the IR spectra. The bands at 1763 (IR) and 1761 cm^{-1} (Raman) are assigned with confidence to the CO stretching vibration, taking into account the spectral region and the reported values for related molecules ($CF_3C(O)CN$: 1765 cm^{-1}; $CH_3OC(O)CN$: 1772 cm^{-1}; HC(O)CN: 1716 cm^{-1}).[18,27,28] A more detailed inspection of the ν(CN) and ν(CO) band shapes reveals shoulders at 2236 and 1770 cm^{-1} in the IR spectrum (gas), which is consistent with the presence of the higher energy *syn* conformer. The rotational isomerism is more evident in the lower frequency modes, where the bands assigned to the *syn* conformer are better resolved.

A medium-intense signal at 1255 cm^{-1} and a weak band at 1218 cm^{-1} in the IR spectrum (gas) are attributed to the antisymmetric C−C−C stretching mode of the *gauche* and *syn* conformers, respectively, by comparison with the calculated band positions and relative intensities. The three strongest gas IR bands at 1179, 1060, and 933 cm^{-1} are assigned to stretching modes of the $ClCF_2$ group of the *gauche* form. The medium-intense band at 904 cm^{-1} is assigned to the most intense IR absorption of the *syn* form. According to calculated displacement vectors, it can be described as an out-of-phase motion of the (O)C−C(N) and C−Cl stretching modes. On the other hand, the weak band at 732 cm^{-1} (IR, gas) featuring a C-type band contour is attributed to the out-of-plane γ(CC(O)C) deformation (*gauche*), usually observed in carbonyl molecules ($CF_3C(O)CN$: 712 cm^{-1}; $CH_3OC(O)CN$: 751 cm^{-1}).[18,27]

Moreover, the *gauche*/*syn* conformational equilibrium also becomes apparent in the liquid phase. The two bands observed at 698 and 645 cm^{-1} in the liquid Raman spectra are assigned to symmetric C−C−C stretching modes of the two conformers. Their large rotamer shifts agree with the predicted values (Table 2). As mentioned above, the C−Cl stretching vibration is strongly mixed with the C−C stretches.

The conformational equilibrium was further studied by the temperature-dependence of the gas IR absorptions in the range between 11 and 92 °C. They are presented in Figure 4 and revealed that the intensity of the bands attributed to the *syn* conformation increases with the temperature, while the intensity of the corresponding bands of the *gauche* form decreases. Although this observation confirms a higher energy of the *syn* form, an accurate estimation of the energy difference between the two conformers was, however, precluded by the mutual overlap of these bands.

In such a case, a matrix-isolation technique is especially appropriate to study the conformational equilibrium, because of the sharpness of the IR absorption bands of species isolated in inert solid matrixes. $ClF_2CC(O)CN$ was isolated in argon (1:2000) and deposited onto the cold matrix support at 15 K. The recorded matrix IR spectrum is shown in Figure 3 (upper trace). In this spectrum, several bands are split by a few wavenumbers due to matrix-site effects. However, no additional conformational splitting was detected, contrary to the results expected from the gas-phase IR spectra. This fact suggests that the gas-phase conformational equilibrium composition might be perturbed during the cooling process. This perturbation can be rationalized in terms of a low energy barrier for the *syn* → *gauche* interconversion, for which the reported value of 3 kcal mol^{-1} can be regarded as an upper limit.[29] Thus, due to a small barrier (probably <3 kcal mol^{-1}), which allows for a rapid *syn* → *gauche* interconversion during the deposition process, only the most

Table 2. Experimental and Calculated Frequencies (cm^{-1}) and Assignment of the Fundamental Vibrational Modes of $ClF_2CC(O)CN$

	experimental				calculated[b,c]		
	IR[a]		Raman[b]				
mode	gas, 298 K	Ar-matrix, 15 K	liquid, 298 K		*gauche*	*syn*	approximate mode description[d]
	3504 w	3498.1					$2\nu_2$
ν_1	2233 m	2232.4	2236 sh 2232	(100)	2341 (42)	2339 (46)	ν(CN)
ν_2	1770 sh					1828 (113)	ν(C═O)
	1763 s	1760.0	1761	(48)	1820 (157)		
ν_3	1255 m	1252.2	1249	(2)	1243 (56)		ν_{as}(C−C−C)
	1218 w					1193 (63)	
ν_4	1179 vs	1177.8	1171	(2)	1162 (179)		$\nu_{as}(CF_2)$
	1121 w					1107 (180)	
ν_5	1060 vs	1054.0	1053	(3)	1053 (228)	1100 (122)	$\nu_s(CF_2)$
ν_6	933 vs	924.1	925	(4)	913 (171)		ν(C−Cl)
	904 m					896 (322)	
ν_7	732 w	729.1	730	(7)	746 (18)	764 (11)	γ(CC(O)C)
ν_8	714 vw		698	(5)		708 (1)	ν_s(C−C−C)
	643 w	640.8	645	(36)	655 (18)		
ν_9	625 w	619.2	624	(6)	626 (21)	617 (4)	δ(C−C−N), $\delta(CF_2)$
ν_{10}	490 vw		493	(3)	502 (2)	412 (2)	$\delta(CF_2)$
ν_{11}	433 vw		437	(27)	428 (3)	447 (2)	ν(C−Cl), ρ(CO)
ν_{12}			388	(7)	387 (8)	383 (19)	$\omega(CF_2)$
ν_{13}			345	(8)	339 (2)	381 (<1)	$\rho(CF_2)$
ν_{14}					279 (8)	293 (4)	δ_{oop}(C−C−N)
ν_{15}			269	(10)	271 (12)	197 (12)	$\tau(CF_2)$
ν_{16}			171	(12)	164 (6)	223 (5)	γ(O−C−C-N)
ν_{17}			137	(22)	128 (2)	126 (2)	$\rho(ClCF_2)$
ν_{18}					43 (0)	26 (0)	$\tau(ClCF_2-C(O))$

[a] Only the most populated Ar-matrix sites are given. Relative band intensities (gas-phase): vs, very strong; s, strong; m, medium strong; w, weak; vw, very week; sh, shoulder. [b] Relative intensities are given in parentheses. [c] B3LYP/6-311+G(3df) calculated IR frequencies (cm^{-1}) and intensities in parentheses (km mol^{-1}). [d] ν, δ, ρ, ω, γ, and τ represent stretching, deformation, rocking, wag, and torsion modes, respectively.

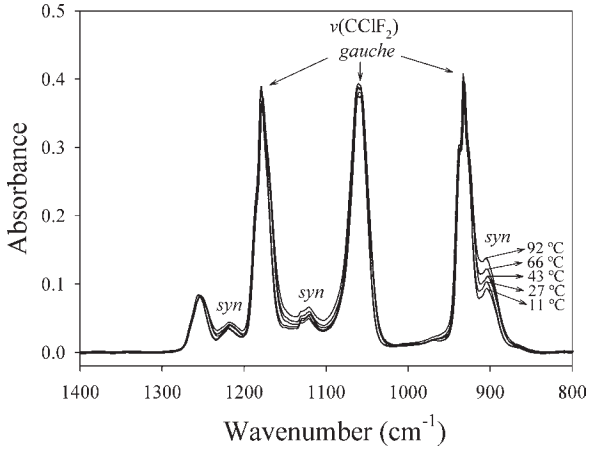

Figure 4. Temperature dependence (11−92 °C) of the C−C and C−F stretching bands of gaseous $ClF_2CC(O)CN$.

stable *gauche* form is detected in the matrix IR spectra at low temperatures. However, the presence of a *gauche*/*syn* conformational equilibrium is strongly supported by (i) calculated relative energies of two rotamers ($\Delta G°_{calc} \leq 1$ kcal mol^{-1}), (ii) the presence of several vibrational modes attributable to a higher-energy conformer, and (iii) their temperature-dependent intensity change in the gas-phase IR spectra.

Gas-Phase Structure Analysis. Gas electron diffraction (GED) was used to determine the gas-phase structure of $ClF_2CC(O)CN$. The structural analysis was performed with the UNEX program.[30] All refinements were performed using two intensity curves (short and long nozzle-to-detector distance) simultaneously. These were obtained by averaging intensity curves measured in independent experiments. For the definition of independent structural parameters and their groups in least-squares refinements, see Table 3. The differences between values of parameters in one group were kept fixed at the calculated values (MP2/cc-pVTZ).

In order to describe the conformational behavior of $ClF_2CC(O)CN$ by means of the GED data, we evaluated them with various models, three of which are outlined here.

The simplest static model used only the pure, most stable *gauche* conformer. The starting values for all parameters and constraints[31] were taken from the B3LYP/6-31G(d) calculation.

dx.doi.org/10.1021/ic201390h |*Inorg. Chem.* 2011, 50, 9650–9659

In this case, the torsion angle O1−C2−C5−Cl6 was refined to give 103.4(55)°. The best total *R* factor achieved with this model was 7.07%.

The next static model was a mixture of two conformers, *gauche* and *syn*. Corresponding structural parameters for both conformers were refined in groups with differences fixed at those values calculated at the B3LYP/6-31G(d) level. The torsion angle O1−C2−C5−Cl6 for the C_s-symmetric *syn* conformer was fixed at 0°; that of the *gauche* conformer was free to refine, resulting in a value of 111.0(30)°. Under these conditions, the conformer ratio was refined simultaneously with the other parameters and led to a value of 90(5)% for the *gauche* conformer. Taking into account that the ESD is not representing the total error, this indicates that it is difficult on the basis of GED to prove the existence of a *syn* conformer at the temperature of this experiment. If there were a substantial abundance of a *syn* conformer, there should be a contribution at 5.1 Å in the radial distribution curve corresponding to the Cl···N distance. Figure 5 shows this curve but also shows no visible contribution in this region. The total *R* factor for this model was 6.95%.

Table 3. Selected GED[a] and Calculated Structural Parameters of *gauche* $ClF_2CC(O)CN$

parameters[b]	GED, r_g	GED, r_e, $\angle_e$	MP2/ cc-pVTZ	B3LYP/ 6-31G(d)
C2−O1	1.204(2)	1.200(2)[1]	1.205	1.194
C2−C3	1.489(7)	1.480(7)[2]	1.465	1.465
C3−N4	1.172(2)	1.168(2)[1]	1.173	1.150
C2−C5	1.534(6)	1.520(6)[3]	1.539	1.550
C5−Cl6	1.761(4)	1.754(4)[4]	1.762	1.788
C5−F7	1.333(2)	1.326(2)[5]	1.325	1.328
C5−F8	1.348(2)	1.341(2)[5]	1.340	1.343
O1−C2−C3		121.8(10)[6]	123.3	122.9
C2−C3−N4		178.8[c]	178.8	178.6
O1−C2−C5		122.3(12)[7]	122.7	122.3
C3−C2−C5		115.9(15)[d]	114.0	114.8
C2−C5−Cl6		108.9(6)[8]	108.1	108.4
C2−C5−F7		110.5(4)[9]	110.2	110.1
C2−C5−F8		109.7(4)[9]	109.4	109.9
Cl6−C5−F7		109.9(2)[10]	110.5	110.1
Cl6−C5−F8		109.1(2)[10]	109.8	109.5
F7−C5−F8		108.7(11)[d]	108.9	108.9
O1−C2−C5−Cl6		110.0[e]	110.0	106.5

[a] The GED results were determined by using a dynamic model. Constraints and potential functions have been taken from MP2/cc-pVTZ calculations. Corrections to the equilibrium structure have been calculated from B3LYP/6-31G(d) harmonic and cubic force fields. [b] Bond lengths (Å) and angles (deg), and 3-times standard deviations are given in parentheses. [c] Fixed parameter. [d] Dependent parameter. [e] Not refined: it corresponds to the minimum on the MP2/cc-pVTZ potential curve calculated with a step of 10.0°.

Finally, a dynamic model was tested. In total, 19 pseudo-conformers, corresponding to different values of the torsion angle O1−C2−C5−Cl6 in the range 0−180° with steps of 10°, were used to construct a dynamic model so that both *gauche* and *syn* conformers were also included. The initial geometrical parameters for each pseudo-conformer were taken from quantum-chemical calculations in order to account for the geometry relaxation in large amplitude torsional motion. The potential function derived from the theoretical calculations was approximated by the following formula:

$$V = V_0 + \sum_i V_i(1 - \cos(i \times \varphi)) \quad (2)$$

In total, three terms in the sum were used. For the MP2/cc-pVTZ potential energy function, the parameters were $V_0 = 1.287$, $V_1 = 0.024$, $V_2 = -1.607$, and $V_3 = 1.613$ kcal mol^{-1}. The refined geometrical parameters and vibrational amplitudes and their groups in the least-squares analysis were all the same as those in the static model except for the O1−C2−C5−Cl6 torsion angle, which was not subject to refining in this dynamic model. The constraints were taken from MP2/cc-pVTZ calculations. The total *R* factor achieved in this refinement was 6.28%. The parameters of the potential function did not refine in an acceptable behavior in the sense that a significant change in their values caused very small changes in the modeled intensity curve. This means that small experimental errors can affect these parameters dramatically. In other words, the refined values of the potential parameters V_i were unreliable and had large standard deviations: $V_1 = -21(15)$, $V_2 = -13(8)$, and $V_3 = -4(3)$ kcal mol^{-1}. In addition, the correlation coefficients between all three refined parameters V_1, V_2, and V_3 were almost 100%. Therefore, it was

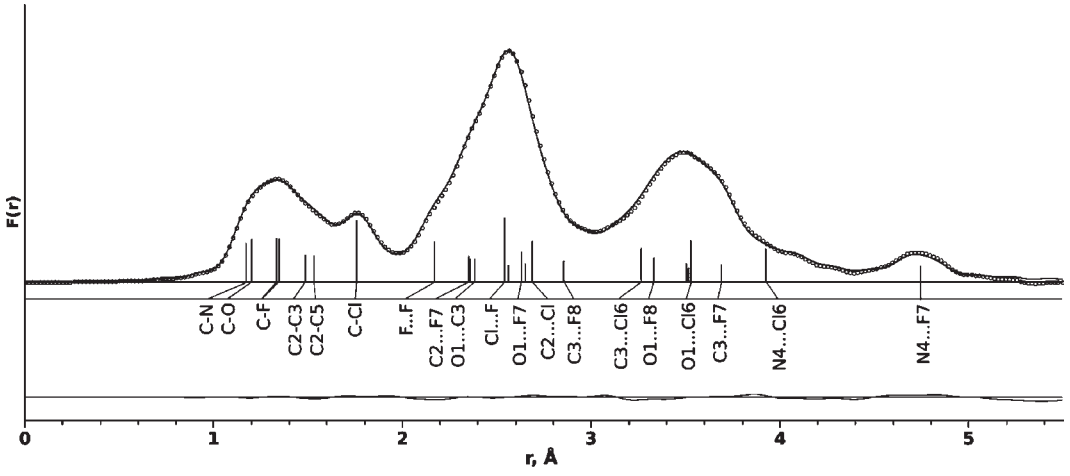

Figure 5. Radial distribution curve, difference (experimental minus theoretical) curve (dots), and model from the GED structure refinement (solid line) of $ClF_2CC(O)CN$. Vertical sticks represent the interatomic distances (selected important ones are labeled).

dx.doi.org/10.1021/ic201390h |*Inorg. Chem.* 2011, 50, 9650–9659

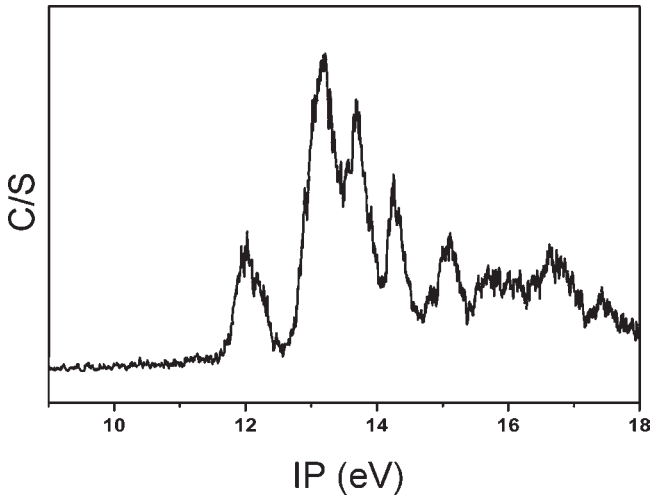

Figure 6. He(I) photoelectron spectrum (PES) of $ClF_2CC(O)CN$.

decided to fix the potential function parameters to their theoretical values. A refinement of the angle C2−C3−N4 gave a value which is close to the theoretical one but with a large standard deviation. Due to that reason, this parameter in the model was also fixed to the theoretical value. Under these conditions, the total *R* factor achieved with the final refined model with theoretical MP2/cc-pVTZ torsional potential was 6.67%. This model was finally considered preferable. The radial distribution functions are shown in Figure 5. The resulting parameter values are presented in Table 3. The agreement of experimental and model molecular intensity curves is shown in the Experimental Section (see below). It should be also noted that, in the case of using constraint values from the B3LYP/6-31G(d) calculations, the total *R* factor at 7.7% was worse.

Photoelectron Spectra. Photoelectron spectroscopy (PES) using He(I) radiation (21.2 eV = 58.4 nm) is a useful technique for studying the valence electronic structure of molecules in combination with theoretical calculations.[32−34] The He(I) photoelectron spectrum of $ClF_2CC(O)CN$ is shown in Figure 6. Outer valence green function (OVGF) calculations were performed to obtain the ionization energies in order to assign the PE spectrum. The experimental vertical ionization potentials (IP), theoretical vertical ionization energies (E_v; OVGF/6-311+G(d)), molecular orbitals (MO), and the corresponding characters of outer valence shells for $ClF_2CC(O)CN$ are listed in Table 4. The OVGF pole strengths, also included in Table 4, are larger than 0.85, which is consistent with a one-electron depiction of ionization and support the use of the OVGF approach.[35] Additionally, the representations of the first eight HOMOs are given in Figure S3 (Supporting Information).

Taking into account the above discussion on the structure of $ClF_2CC(O)CN$, it is concluded that the *gauche* conformer is the preferred one in the gas phase, and it is assumed that the observed spectrum mainly arises from the energetically most favorable isomer. In addition, theoretical calculations (OVGF/6-311+G(d)) for the two isomers do not predict appreciable differences in the ionization energies with respect to the experimental resolution of 30 meV (∼ 240 cm^{-1}).

The vertical ionization energies observed in the photoelectron spectrum of $ClF_2CC(O)CN$ agree with the calculated values of the OVGF method. The first band in the photoelectron spectrum is centered at 12.00 eV and can be attributed to the ionization

Table 4. Experimental and Calculated Ionization Energies[a] and MO Characters for $ClF_2CC(O)CN$

band	exptl. IP	calcd. E_v[b,c]	MO	character
1	12.00	12.40 (0.904)	34	n_O
2	13.19	13.09 (0.897)	33	n_{Cl}
3	13.71	13.35 (0.903)	32	n_{Cl}
4	13.91	13.82 (0.898)	31	$\pi_{b\ (CN)}$
5	14.24	14.03 (0.900)	30	$\pi_{b\ (CN)}$
6	15.10	15.27 (0.894)	29	$\pi_{b\ (C=O)}$

[a] Energies [eV]. [b] OVGF from geometries at the B3LYP/6-31+G(d) level. [c] Pole strength in parentheses.

process from the highest occupied molecular orbital (HOMO), corresponding to the nonbonding orbital on the oxygen atom (n_O). This ionization energy was also reported at 11.21, 11.65, and 13.20 eV for $CH_3C(O)CN$,[23] $CH_3OC(O)CN$,[36] and FC(O)CN,[22] respectively, showing the intermediate inductive effect of the $ClCF_2$ group (with respect to CH_3 and F) and the dependence of the IP (photo ionization energies) on the electronegativity of the groups linked to C═O.

The second and third ionization bands are observed at 13.19 and 13.71 eV. They are attributed to the ejection of electrons from the two nonbonding orbitals of the chlorine atom (n_{Cl}). These IP were reported at 12.60 eV for the degenerated n_{Cl} orbitals of the related molecule $HClCF_2$ (C_s symmetry),[37] while the calculated OVGF values (13.35 and 13.82 eV) agree closely, supporting the present assignment. The following two ionization bands observed at 13.91 and 14.24 eV are attributed to ionization from the π-type bonding orbitals of the cyano group, $\pi_{b(CN)}$, considering the calculated values and the coincidence with other carbonyl−cyanide molecules such as $CH_3C(O)CN$ (13.09 and 13.82 eV),[23] $CH_3OC(O)CN$ (13.04 and 13.31),[36] and FC(O)CN (13.90 and 14.14 eV).[22] The last well-resolved band at 15.10 eV may have originated from the energy ionization of the π-type bonding orbital of the carbonyl group, $\pi_{b(C=O)}$, as reported for the similar molecule acetyl cyanide (15.03 eV). However, it is also possible that this process originates from the nonbonding orbital on the nitrogen atom (n_N) taking into account the previously discussed reports for FC(O)CN and HC(O)CN.[22,38]

To analyze the nature of the cation formed on the first ionization process, UB3LYP/6-311+G(3df) calculations were performed. The results show that the atomic charges (Table S1, Supporting Information) are mostly delocalized throughout the molecule, with a significant proportion localized at the oxygen and chlorine atoms, according to the main character of the first ionization energies discussed above. After the ionization process, the C_1 molecular symmetry is maintained, and some structure parameters are significantly affected: the C2−C5 bond is lengthened by 0.46 Å, while the C═O double bond is shortened by 0.04 Å relative to the ground state. Consequently, the vibrational calculations performed for the cationic form result in a blue shift of 241 cm^{-1} for the ν(C═O) and a large red shift of 648 cm^{-1} in the ν(C2−C5), compared with the neutral form.

Photoionization Mass Spectrum. The ultraviolet photoionization mass spectrum (PIMS) of $ClF_2CC(O)CN$ was determined together with the photoelectron spectra, and it is shown in Figure 7. The PIMS confirmed the identity of the sample. However, the analysis of the results becomes more useful when it is combined with PES and theoretical results. The spectrum of $ClF_2CC(O)CN$ mainly shows four peaks: CF_2^+, $C(O)CN^+$,

dx.doi.org/10.1021/ic201390h |*Inorg. Chem.* 2011, 50, 9650–9659

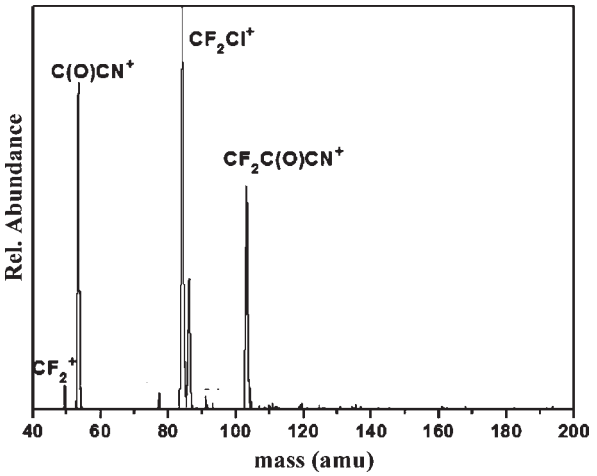

Figure 7. He(I) photoionization mass spectrum (PIMS) of $ClF_2CC(O)CN$.

$ClCF_2^+$, and $CF_2C(O)CN^+$. To evaluate the dissociation pathways, the adiabatic ionization (I_a) of $ClF_2CC(O)CN$ and the energy of the identified fragments were obtained by quantum-chemical calculation (Table S2, Supporting Information). They are required to build the energy diagrams of the dissociation pathway shown in Figure 8. Assuming the absence of any significant energy barriers, the fragmentation distribution would be governed by the relative energies of the various product states.[39]

The adiabatic ionization energy (I_a) calculated for $ClF_2CC(O)CN$ at the UB3LYP/6-311+G(3df) approximation is 11.15 eV. The molecular geometry of the involved radical-cation $ClF_2CC(O)CN^{\bullet+}$ was predicted to be similar to that of the parent $ClF_2CC(O)CN$ (C_1 symmetry), with the exception of a longer C2−C5 bond (Δ = 0.46 Å). This result suggests that the parent ion probably dissociates at the C2−C5 single bond to form the ion/radical pairs $ClF_2C^+ + C(O)CN^{\bullet}$ or $ClF_2C^{\bullet} + C(O)CN^+$. The dissociation pathway profile, displayed in Figure 8, shows that the energy for the dissociation of the parent ion to the $ClF_2C^+ + C(O)CN^{\bullet}$ pair (0.41 eV) is lower than to the $ClCF_2^{\bullet} + C(O)CN^+$ pair (0.88 eV), which agrees with the fact that the ClF_2C^+ ion corresponds to the most intense signal in the PIMS spectrum. However, the $C(O)CN^+$ ion was also detected in high yield, favored by the low calculated dissociation energy. Moreover, the direct dissociation from the parent to the $F_2CC(O)CN^+ + Cl^{\bullet}$ pair is characterized by a higher dissociation energy (1.54 eV), and therefore a lower intense $CF_2C(O)CN^+$ signal was observed. On the other hand, the weak signal corresponding to the CF_2^+ ion agrees with the higher dissociation energy corresponding to the formation of the $CF_2^+ + Cl^{\bullet} + C(O)CN^{\bullet}$ species.

UV Fine Structure. The fine structure developed in the UV spectrum (Figure S2, Supporting Information) provides a selective vibrational view of the relevant excited electronic state of the $ClF_2CC(O)CN$ molecule. The interpretation of this vibronic structure is, however, complicated by a number of factors. First, the parent molecule and its excited state have only low symmetry, and at wavenumbers below about 1500 cm^{-1}, the vibrational modes are not expected to be described in terms of a single symmetry coordinate. Although it is reasonable to expect that the most prominent component of a vibrational progression is due to a vibrational transition which suffers a major change of wavenumber as a result of the transition in question, the relatively modest resolution of our spectra may well hide more than one progression, and it does not follow that the interval in the progression is necessarily the wavenumber of a single fundamental vibration of the electronic excited state. Nevertheless, the vibronic structure can, in principle, give important indications to the nature of that state and to the excitation process with which it is associated.

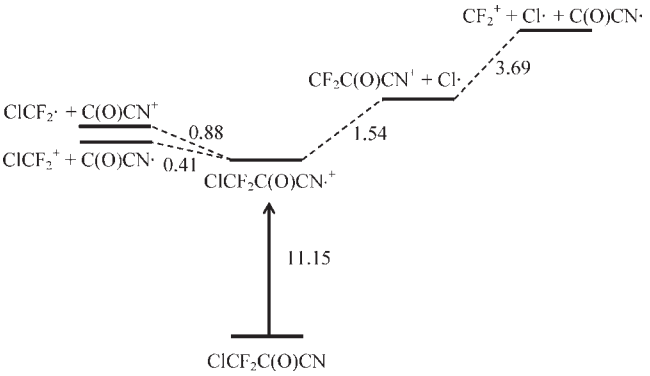

Figure 8. Schematic energy profile [eV] of ionization and possible dissociation pathways for $ClF_2CC(O)CN$ calculated at the B3LYP/6-311+G(3df) level.

The fine structure is dominated by a progression with ν_o = 1060 ± 30 cm^{-1}. In the absence of more positive information, it is plausible that the interval represents a vibrational mode of a particular excited electronic state of $ClF_2CC(O)CN$ involving, at least in part, the ν(C═O) vibration. It would then signal a dramatic reduction in bond order of the original C═O bond brought about by the electronic promotion, with a corresponding decrease in force constant and wavenumber of the C═O stretching vibration, in agreement with the expected behavior of an $n \rightarrow \pi^*$ (CO) electronic transition.

■ CONCLUSION

$ClF_2CC(O)CN$ is a new eight-atom molecule with potential applications in preparative chemistry according to its nature and properties. This compound has been fully characterized in terms of its physical, spectroscopic, and structural data. It adopts two conformations in the gas and liquid phases with C_1 (*gauche*) and C_s (*syn*) symmetry according to vibrational spectroscopic data and quantum chemical calculations. Nevertheless, gas electron diffraction measurements at ambient temperature are not conclusive regarding the existence of a *syn* conformer. However, the high flexibility of the molecule concerning the torsional mode requires a dynamic model to fit the electron diffraction data in order to reflect large amplitude motions.

The electronic structure of $ClF_2CC(O)CN$ was analyzed. The first vertical ionization energy is at 12.00 eV and corresponds to the leaving electrons mainly localized on the lone-pair orbital of the oxygen atom. After ionization, the cationic radical formed, [$ClF_2CC(O)CN^{\bullet+}$], keeps the structure with C_1 symmetry; however, the ClC−C(O) bond elongates by 0.46 Å, which agrees with the proposed main dissociation processes ($ClF_2C^+ + C(O)CN^{\bullet}$).

■ EXPERIMENTAL SECTION

Synthesis. $ClF_2CC(O)CN$ was synthesized by the reaction of difluorochloroacetyl chloride, $ClCF_2C(O)Cl$, with excess of silver

dx.doi.org/10.1021/ic201390h |*Inorg. Chem.* 2011, 50, 9650–9659

cyanide, AgCN. For this purpose 1.5 g $ClCF_2C(O)Cl$ were distilled into a 250 mL glass vessel containing 2.5 g of dry AgCN and provided with a Young valve. The reaction was carried out in vacuum during 1.5 h at 200 °C. Purification of the product was performed by trap-to-trap distillations with traps held at −25, −100, and −196 °C. $ClF_2CC(O)CN$ was isolated in the trap at −100 °C together with a small amount of difluorochloroacetyl chloride, which was further separated by slow vacuum distillation. Removing $ClCF_2C(O)Cl$ is arduous because the similarity of the vapor pressures. To ensure the total consumption of $ClCF_2C(O)Cl$ an excess of AgCN was added (a big reaction vessel should be used taking into account that the reaction take place on the surface of the AgCN (200 °C)). The final yield was 68% (0.95 g).

Silver cyanide was prepared from $AgNO_3$ and KCN, while $ClCF_2C(O)Cl$ by chlorination of the corresponding acid, $ClCF_2C(O)OH$, with PCl_5.[40]

Instrumentation and Procedure. *a. General Procedure.* Volatile materials were manipulated in a glass vacuum line equipped with a capacitance pressure gauge (221 AHS-1000, MKS Baratron, Burlington, MA), three U-traps, and valves with PTFE stems (Young, London, U.K.). The vacuum line was connected to an IR cell (optical path length 200 mm, Si windows 0.5-mm-thick) placed in the sample compartment of a Bruker Vector 25 FTIR spectrometer. This arrangement allows for recording the course of the reactions and the purification processes. The pure compound was stored in flame-sealed glass ampules under liquid nitrogen in a Dewar vessel. The ampules were opened with an ampule key[56] at the vacuum line. An appropriated amount was taken out for the experiments, and then they were flame-sealed again. The vapor pressures of the sample were measured in a small vacuum line equipped with a calibrated capacitance pressure gauge (MKS Baratron, AHS-100) and a small sample reservoir.

The melting point of $ClF_2CC(O)CN$ was determined by condensing 100 mg of the sample in vacuo onto the bottom of a small L-shaped tube connected to a vacuum line. Then, the temperature was increased at a rate of about 1 °C min^{-1} starting at −100 °C (cold ethanol bath). The solid melts at −75 °C to a colorless liquid. The vapor pressure of the liquid was measured, in a similar way, in the temperature range between −60 and 0 °C.

b. Vibrational Spectroscopy. Infrared gas spectra were recorded on a Bruker Vector 25 spectrometer, with a resolution of 2 cm^{-1} in the range from 4000 to 400 cm^{-1}, using a glass cell with Si windows and optical path length of 200 mm.

Temperature-dependent infrared spectra were measured on a Bruker IFS 66v/S FTIR spectrometer (resolution: 2 cm^{-1}) using a KBr beam splitter and a mercury cadmium telluride (MCT) detector in the region of 4000−530 cm^{-1}. For this purpose, a double-walled gas cell with an optical path length of 200 mm, equipped with Si windows (0.5 mm thick), a pressure gauge (221 AHS-100, MKS Baratron, Burlington, MA), and a Pt-100 temperature sensor, was placed in the evacuated sample compartment of the spectrometer. The temperature was controlled by cold and warm nitrogen gas streams at high flow rates. Up to five IR spectra for gaseous $ClF_2CC(O)CN$ at different temperatures, in the range from 11 to 92 °C, were recorded. For each of these temperatures, the cell was refilled with a new sample, and a new background was recorded.

Raman spectra of the neat liquid at room temperature were measured in flame-sealed capillaries (3 mm o.d.) on a Bruker RFS 106/S spectrometer, equipped with a 1064 nm Nd:YAG laser, in the region from 4000 to 100 cm^{-1} using 2 cm^{-1} of resolution.

c. Matrix Isolation Experiments. For matrix isolation experiments, $ClF_2CC(O)CN$ was diluted with argon in a ratio of 1:2000 in a 1 L stainless-steel storage container, and then small amounts of the mixture were deposited within 10 min onto the cold matrix support (16 K, Rh-plated Cu-block) under high vacuum conditions. Temperature-dependent experiments were carried out by passing the gaseous sample−Ar mixtures through a quartz nozzle (1 mm i.d.), heated over a length

Table 5. Details of the GED Experiment

parameter	short camera distance	long camera distance
nozzle-to-film distance, mm	250.0	500.0
accelerating voltage, kV	59.997(1)	60.001(1)
fast electrons current, μA	0.9	1.3
electron wavelength, Å	0.048733	0.048597
nozzle temperature, K	293	293
residual gas pressure,[a] bar	1.6×10^{-5}	1.8×10^{-5}
exposure time, s	30,46	30,47
used s range, $Å^{-1}$	7.0−33.0	3.0−17.4
number of inflection points[b]	5	4
R_{exp},[c] %	7.3	5.8

[a] During the measurement. [b] Number of inflection points on the background line. [c] Experimental R factor.[55]

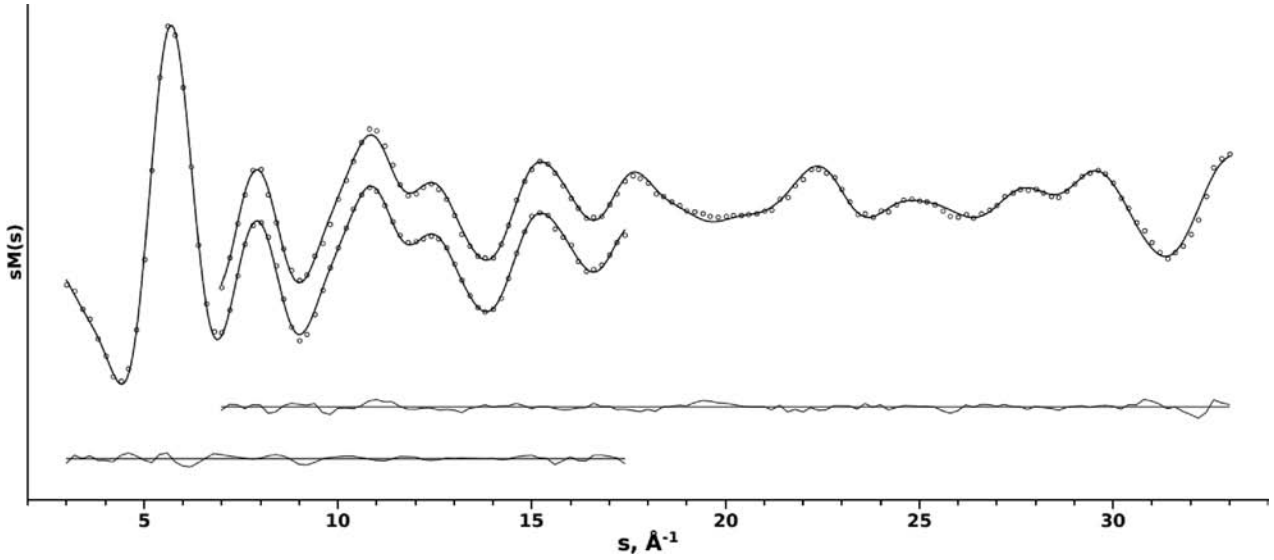

Figure 9. Experimental (dots) and difference (experimental minus theoretical; solid line) molecular scattering intensity curves for $ClF_2CC(O)CN$.

dx.doi.org/10.1021/ic201390h |Inorg. Chem. 2011, 50, 9650–9659

of ~10 mm with a platinum wire (0.25 mm o.d.) prior to deposition on the matrix support. The nozzle was held at 210 and 300 °C.

IR spectra of matrix isolated samples were recorded in reflectance mode on a Bruker IFS 66v/S spectrometer using a transfer optic. An MCT detector and a KBr/Ge beam splitter were used in the wavenumber range 5000−530 cm^{-1}. For the spectra with apodized resolutions of 0.25 cm^{-1}, 200 scans were added. More details of the matrix apparatus are given elsewhere.[41]

d. UV Spectroscopy. The UV−visible spectrum of gaseous $ClF_2CC(O)CN$ was recorded using a glass cell equipped with quartz windows (10 cm optical path length) on a Lambda EZ210 UV/vis spectrometer (Perkin-Elmer). Measurements were carried out in the spectral region from 190 to 700 nm with a sampling interval of 1.0 nm, a scan speed of 200 nm min^{-1}, and a slit width of 2 nm.

e. NMR Spectroscopy. For ^{13}C and ^{19}F NMR spectra, pure samples were flame-sealed in thin-walled 4 mm o.d. tubes and placed into 5 mm NMR tubes. The NMR spectra were recorded on a Bruker Avance 400 spectrometer at 100.6 and 376.5 MHz, respectively. The samples were held at 25 °C, and C_6D_6 was used as an external lock and reference.

f. Quantumchemical Calculations. Quantum chemical calculations were performed using the program package Gaussian 03.[42] Scans of the potential energy surface, structure optimizations, and vibrational frequencies of $ClF_2CC(O)CN$ have been carried out applying ab initio (MP2),[43] density functional theory (B3LYP),[44−47] and complete basis set CBS-QB3 methods.[48,49] To assign the PES of $ClF_2CC(O)CN$, we applied the OVGF approach with a 6-311+G(d) basis set, which includes correlation effects of the self-energy to the molecules to give accurate results of the vertical ionization energies.[35] Molecular orbital plots were generated with the Gauss View program by using the 0.05 isodensity.

g. Photoelectron and Photoionization Mass Spectroscopy. The equipment used in this work has been described previously.[50,51] The photoelectron and photoionization mass spectrometer consists of two parts: the double-chamber UPS-II machine and a time-of-flight mass spectrometer. The PES was recorded in a double-chamber UPS-II with a resolution of about 30 meV, as indicated by the Ar^+ ($^2P_{3/2}$) photoelectron band. Experimental vertical ionization energies (IP) were calibrated by the simultaneous addition of a small amount of argon and methyl iodide to the sample. Mass analysis of ions was performed with the time-of-flight mass analyzer mounted directly to the photoionization point. The relatively soft ionization is provided by single-wavelength He I radiation. The PE and PIM spectra can be recorded within seconds of each other under identical conditions.

h. Gas Electron Diffraction. The electron diffraction patterns were recorded on the heavily improved Balzers Eldigraph KD-G2 gas-phase electron diffractometer[52] at the University of Bielefeld. The experimental details are presented in Table 5. In total, two images for each, the long and short nozzle-to-plate camera distances, were measured on Fuji BAS-IP MP 2025 imaging plates. The plates with the diffraction patterns were scanned using a calibrated Fuji BAS-1800II scanner. The intensity curves (Figure 9) were obtained by applying the method described earlier.[53] Sector function and electron wavelengths were estimated using the method described in ref 54, which is against benzene diffraction patterns, recorded along with the substance under investigation. The quality of the experimental data was estimated by means of experimental *R* factors[55] (see Table 5) for long and short camera distances, respectively.

In order to calculate amplitudes of vibrations and curvilinear corrections used in the gas-phase electron diffraction refinements, analytical quadratic and numerical cubic force fields were calculated for both *gauche* and *syn* conformers employing the B3LYP/6-31G(d) approximation. The mean square amplitudes and vibrational corrections to the equilibrium structure were calculated with the SHRINK program.[56−59]

■ ASSOCIATED CONTENT

Ⓢ Supporting Information. ^{19}F and ^{13}C NMR spectra of $ClF_2CC(O)CN$ (Figure S1), UV−vis spectrum of gaseous $ClF_2CC(O)CN$ (Figure S2), characters of the highest occupied molecular orbitals of $ClF_2CC(O)CN$ (Figure S3), Mulliken atomic charges for the molecular and cation-radical forms of $ClF_2CC(O)CN$ calculated with the UB3LYP/6-311+G(d) approximation, and the calculated total and ionization energies of $ClF_2CC(O)CN$ and its fragments. This material is available free of charge via the Internet at http://pubs.acs.org.

■ AUTHOR INFORMATION

Corresponding Author
*E-mail: carlosdv@quimica.unlp.edu.ar.

■ ACKNOWLEDGMENT

The authors thank the Deutsche Forschungsgemeinschaft (DFG), the Fonds der Chemischen Industrie, the Alexander von Humboldt Stiftung, the Deutscher Akademischer Austauschdienst (DAAD, Regional Program of Chemistry for the Argentina supporting Latin-American students to do their Ph.D. in La Plata), Agencia Nacional de Promoción Científica y Técnica (ANPCYT), Consejo Nacional de Investigaciones Científicas y Técnicas (CONICET), Comisión de Investigaciones de la Provincia de Buenos Aires (CIC), Facultad de Ciencias Exactas, Universidad Nacional de La Plata (UNLP) and Departamento de Ciencias Básicas de la Universidad Nacional de Luján, Bergische Universität Wuppertal, and Universität Bielefeld for financial support. S.E.U especially thanks Deutscher Akademischer Austauschdienst Germany (DAAD) for an equipment grant and financial support.

■ REFERENCES

(1) Hünig, S.; Schaller, R. *Angew. Chem., Int. Ed. Engl.* **1982**, *21*, 36–49.
(2) Murahashi, S.; Naota, T.; Nakajima, N. *J. Org. Chem.* **1986**, *51*, 898–901.
(3) Santelli, M.; El Abed, D.; Jellal, A. *J. Org. Chem.* **1986**, *51*, 1199–1206.
(4) Potts, K. T. *J. Org. Chem.* **1961**, *26*, 4719–4721.
(5) Borch, R. F.; Levitan, S. R.; Van-Catledge, F. A. *J. Org. Chem.* **1972**, *37*, 726–729.
(6) Baek, H. S.; Lee, S. J.; Yoo, B. W.; Ko, J. J.; Kim, S. H.; Kim, J. H. *Tetrahedron Lett.* **2000**, *41*, 8097–8099.
(7) Okimoto, M.; Itoh, T.; Chiba, T. *J. Org. Chem.* **1996**, *61*, 4835–4837.
(8) Burger, A.; Hornbaker, E. D. *J. Am. Chem. Soc.* **1952**, *74*, 5514–5514.
(9) Midland, M. M.; Lee, P. E. *J. Org. Chem.* **1985**, *50*, 3237–3239.
(10) Macías-Ruvalcaba, N. A.; Evans, D. H. *J. Org. Chem.* **2006**, *72*, 589–594.
(11) Oaksmith, J. M.; Peters, U.; Ganem, B. *J. Am. Chem. Soc.* **2004**, *126*, 13606–13607.
(12) De Pol, S.; Zorn, C.; Klein, C. D.; Zerbe, O.; Reiser, O. *Ang. Chem. Int. Ed.* **2004**, *43*, 511–514.
(13) Schmitt, M. A.; Weisblum, B.; Gellman, S. H. *J. Am. Chem. Soc.* **2004**, *126*, 6848–6849.
(14) Nakao, Y.; Hirata, Y.; Hiyama, T. *J. Am. Chem. Soc.* **2006**, *128*, 7420–7421.
(15) Hirata, Y.; Inui, T.; Nakao, Y.; Hiyama, T. *J. Am. Chem. Soc.* **2009**, *131*, 6624–6631.

(16) Rondla, N. R.; Levi, S. M.; Ryss, J. M.; Vanden Berg, R. A.; Douglas, C. J. *Org. Lett.* **1986**, *13*, 1940–1943.
(17) Hirata, Y.; Yada, A.; Morita, E.; Nakao, Y.; Hiyama, T.; Ohashi, M.; Ogoshi, S. *J. Am. Chem. Soc.* **2010**, *132*, 10070–10077.
(18) Lidy, W.; Sundermeyer, W. *Chem. Ber.* **1976**, *109*, 1491–1496.
(19) Patton, R. H.; Simons, J. H. *J. Am. Chem. Soc.* **1957**, *79*, 894–895.
(20) Duncan, D.; Livinghouse, T. *Organometallics* **1999**, *18*, 4421–4428.
(21) Liu, Y.; Yan, B. *Organometallics* **2005**, *25*, 544–547.
(22) Von Niessen, W.; Fougère, S. G.; Janvier, D.; Klapstein, D. *J. Mol. Struct.* **1992**, *265*, 133–142.
(23) Katsumata, S.; Tabayashi, K.; Sugihara, T.; Kimura, K. *J. Electron Spectros. Relat. Phenom.* **2000**, *113*, 49–55.
(24) Erben, M. F.; Boese, R.; Willner, H.; Della Védova, C. O. *Eur. J. Org. Chem.* **2007**, *2007*, 4917–4926.
(25) Furlan, A.; Scheld, H. A.; Huber, J. R. *J. Phys. Chem. A* **2000**, *104*, 1920–1929.
(26) Ramos, L. A.; Ulic, S. E.; Romano, R. M.; Erben, M. F.; Lehmann, C. W.; Bernhardt, E.; Beckers, H.; Willner, H.; Della Védova, C. O. *Inorg. Chem.* **2010**, *49*, 11142–11157.
(27) Durig, J. R.; Groner, P.; Drew, A. S.; Guirgis, G. A.; van der Veken, B. J. *J. Raman Spectrosc.* **1995**, *26*, 43–55.
(28) Lewis-Bevan, W.; Gaston, R. D.; Tyrrell, J.; Stork, W. D.; Salmon, G. L. *J. Am. Chem. Soc.* **1992**, *114*, 1933–1938.
(29) Bodenbinder, M.; Ulic, S. E.; Willner, H. *J. Phys. Chem.* **1994**, *98*, 6441–6444.
(30) Vishnevskiy, Y. V. UNEX version 1.5. http://molstruct.chemport.ru (accessed Aug 2011).
(31) Mitzel, N. W.; Rankin, D. W. H. *Dalton Trans.* **2003**, 3650–3662.
(32) Yao, L.; Ge, M. F.; Wang, W.; Zeng, X.; Sun, Z.; Wang, D. *Inorg. Chem.* **2006**, *45*, 5971–5975.
(33) Zeng, X.; Ge, M.; Sun, Z.; Wang, D. *Inorg. Chem.* **2005**, *44*, 9283–9287.
(34) Zeng, X.; Liu, X.; Sun, X.; Ge, X.; Zhang, X.; Ai, X.; Meng, X.; Zheng, X.; Wang, X. *Inorg. Chem.* **2004**, *43*, 4799–4801.
(35) Ortiz, J. V. *J. Chem. Phys.* **1988**, *89*, 6348–6352.
(36) Zeng, X.-Q.; Ge, M.-F.; Du, L.; Sun, Z.; Wang, D.-X. *J. Mol. Struct.* **2006**, *800*, 62–68.
(37) Cvitas, T.; Gusten, H.; Klasinc, L. *J. Chem. Phys.* **1977**, *67*, 2687–2691.
(38) Vallée, Y.; Ripoli, J.; Lacombe, S.; Pfister-Guillouzo, G. *J. Chem. Res.* **1990**, 401–412.
(39) Shengrui, T.; Lin, D.; Li, Y.; Maofa, G.; Carlos, O. D. V. *Eur. J. Inorg. Chem.* **2008**, *2008*, 3987–3995.
(40) Corley, R. S.; Cohen, S. G.; Simon, M. S.; Wolosinski, H. T. *J. Am. Chem. Soc.* **1956**, *78*, 2608–2610.
(41) Schnöckel, H. G.; Willner, H. *Infrared Raman Spectrosc., Methods Appl.* **1994**, 297.
(42) Frisch, M. J. et al. *Gaussian 03*; Gaussian Inc.: Wallingford,CT, 2004.
(43) Møller, C.; Plesset, M. S. *Phys. Rev.* **1934**, *46*, 618.
(44) Becke, A. D. *J. Chem. Phys.* **1993**, *98*, 5648–5652.
(45) Lee, C.; Yang, W.; Parr, R. G. *Phys. Rev. B* **1988**, *37*, 785.
(46) Perdew, J. P.; Burke, K.; Ernzerhof, M. *Phys. Rev. Lett.* **1996**, *77*, 3865.
(47) Perdew, J. P.; Burke, K.; Ernzerhof, M. *Phys. Rev. Lett.* **1997**, *78*, 1396.
(48) Montgomery, J. J. A.; Frisch, M. J.; Ochterski, J. W.; Petersson, G. A. *J. Chem. Phys.* **1999**, *110*, 2822–2827.
(49) Montgomery, J. A.; Frisch, M. J.; Ochterski, J. W.; Petersson, G. A. *J. Chem. Phys.* **2000**, *112*, 6532–6542.
(50) Zhao, H.; Wang, D.; Xu, G. *J. Anal. Instrumen.* **1992**, *4*, 23.
(51) Willet, G. D. Ph.D. Thesis, La Trobe University, Australia, 1977.
(52) Berger, R. J. F.; Hoffmann, M.; Hayes, S. A.; Mitzel, N. W. Z. *Naturforsch. B* **2009**, *64b*, 1259–1268.
(53) Vishnevskiy, Y. V. *J. Mol. Struct.* **2007**, *833*, 30–41.
(54) Vishnevskiy, Y. V. *J. Mol. Struct.* **2007**, *871*, 24–32.
(55) Vishnevskiy, Y. V.; Shishkov, I. F.; Khristenko, L. V.; Rykov, A. N.; Vilkov, L. V.; Oberhammer, H. *Russ. J. Phys. Chem.* **2005**, *79*, 1537–1547.
(56) Sipachev, V. A. *J. Mol. Struct.* **2004**, *693*.
(57) Sipachev, V. A. *J. Mol. Struct.* **2001**, *567−568*, 67–72.
(58) Sipachev, V. A. *Struct. Chem.* **2000**, *11*, 167–172.
(59) Sipachev, V. A. *THEOCHEM* **1985**, *121*, 143–151.